Unique Piezoelectric Properties of the Monoclinic Phase in Pb(Zr,Ti)O_{3} Ceramics: Large Lattice Strain and Negligible Domain Switching

Longlong Fan, Jun Chen, Yang Ren, Zhao Pan, Linxing Zhang, and Xianran Xing

Phys. Rev. Lett. **116**, 027601 — Published 15 January 2016

DOI: 10.1103/PhysRevLett.116.027601

Unique Piezoelectric Properties of the Monoclinic Phase in $Pb(Zr,Ti)O_3$ Ceramics: Large Lattice Strain and Negligible Domain Switching

Longlong Fan[a], Jun Chen[a,b,*], Yang Ren[c], Zhao Pan[a], Linxing Zhang[a], and Xianran Xing[a,*]

[a] Department of Physical Chemistry, University of Science and Technology Beijing, Beijing 100083, China

[b] Beijing Key Laboratory of Special Melting and Preparation of High-End Metal Materials, University of Science and Technology Beijing, Beijing 100083, China

[c] X-ray Science Division, Advanced Photon Source, Argonne National Laboratory, Argonne, IL 60439 USA

* junchen@ustb.edu.cn or xing@ustb.edu.cn.

Abstract

The origin of the excellent piezoelectric properties at the morphotropic phase boundary is generally attributed to the existence of a monoclinic phase in various piezoelectric systems. However, there exist no experimental studies which reveal the role of the monoclinic phase in the piezoelectric behavior in phase-pure ceramics. In this work, a single monoclinic phase has been identified in $Pb(Zr,Ti)O_3$ ceramics at room temperature by in-situ high-energy synchrotron X-ray diffraction and its response to electric field has been characterized for the first time. Unique piezoelectric properties of the monoclinic phase in terms of large intrinsic lattice strain and negligible domain switching have been observed. The extensional strain constant d_{33} and the transverse strain constant d_{31} are calculated to be 520 and -200 pm/V, respectively. These large piezoelectric coefficients are mainly due to the large intrinsic lattice strain, with very little extrinsic contribution from domain switching. The unique properties of the monoclinic phase provide new insights into the mechanisms responsible for the piezoelectric properties at the morphotropic phase boundary.

$Pb(Zr_xTi_{1-x})O_3$ (PZT100x) ceramics at the morphotropic phase boundary (MPB), with the MPB region where tetragonal and rhombohedral phases coexist [1,2], exhibit excellent piezoelectric and ferroelectric properties and have been widely investigated for understanding the fundamentals of piezoelectricity and related phenomena. In 1999, Noheda *et al.* first observed the low symmetry monoclinic phase in the PZT52 powder at 20 K [3]. Thereafter, the existence of the monoclinic phase was revealed in other $PbTiO_3$-based ferroelectrics near the MPB [4-7]. The existence of the monoclinic phase provides us a new insight into the mechanism of excellent piezoelectric properties for those compositions near the MPB. From the crystallographic point of view, the monoclinic phase serves as an intermediate state during the polarization rotation between tetragonal (polar axis along $<001>_{pc}$) and rhombohedral (polar axis along $<111>_{pc}$) phases [8-11]. First-principle calculations suggest that the tetragonal and rhombohedral phases are linked by the monoclinic phase with large piezoelectric effect [1,12,13]. In addition, the tetragonal and rhombohedral phases around the MPB were claimed to display an outstanding piezoelectric response along the monoclinic plane. For example, the d_{33} of the rhombohedral phase and the d_{15} of the tetragonal phase are large along the $<001>_{PC}$ direction [14-16].

Although the role of the monoclinic phase in the piezoelectric mechanism has been investigated by means of first-principles calculations, the piezoelectric mechanism of the monoclinic phase has not been experimentally explored in ceramics. Therefore, it is important to experimentally examine the poling process of a single monoclinic phase at room temperature. However, the monoclinic phase generally coexists with either tetragonal or rhombohedral phase at room temperature [8,17-19]. For instance, in the PZT ceramics near the MPB, an electric field can result in phase transition from either tetragonal or rhombohedral phase to monoclinic phase. However, after unloading the applied electric field, the monoclinic phase reverts back to the tetragonal or the rhombohedral phase [10,17]. This makes it challenging to obtain information on the structure and domain mobility of the monoclinic phase, due to the peak overlapping resulting from phase coexistence of monoclinic, tetragonal, and rhombohedral phases. In particular, by applying an electric field, the shift of rhombohedral $(200)_{PC}$ and tetragonal $(111)_{PC}$ reflections around the MPB is remarkably superimposed on the monoclinic plane [8,20]. If a single monoclinic phase could be experimentally observed at room temperature in PZT ceramics, then the response of the monoclinic phase can be directly studied. Especially, the piezoelectric contributions of intrinsic lattice strain and extrinsic domain switching from the monoclinic phase can be extracted. The results would be helpful to elucidate the role of the monoclinic phase in the piezoelectric mechanism and for the design of new piezoelectric materials with high performance.

In this letter, a single monoclinic phase in the PZT53.5 ceramics at room temperature has been identified by means of in-situ high-energy synchrotron X-ray diffraction (SXRD). The single monoclinic phase is completely transformed from the tetragonal phase during electrical loading and remains also after the removal of the electric field. The in-situ studies of structural refinement and texture analysis have been successfully employed on the single monoclinic phase, which has revealed the different contributions of the intrinsic lattice strain and the extrinsic domain mobility to the macro piezoelectric performance. The present work provides direct experimental evidence for the character of the monoclinic phase in ceramics, namely large intrinsic lattice strain but negligible extrinsic domain switching.

The $Pb(Zr_{0.535}Ti_{0.465})O_3$ (PZT53.5) ceramic samples were prepared using the solid state reaction method. In order to reveal the phase structure of bulk ceramics, we used high-energy synchrotron X-ray radiation, which can penetrate thick PZT ceramics. The transmission mode was adopted in order to investigate the bulk response of PZT53.5 ceramic under electric field and avoid surface layer effects inherent in the lower energy symmetric reflection geometry. The in-situ high-energy SXRD investigations on PZT53.5 under applied electric field were performed at 11-ID-C at Advanced Photon Source (APS). More experimental details are given in the Supplemental Material [21].

It is well-known that piezoelectric and ferroelectric properties are correlated with the phase structure of ceramics. Differently from the powder diffraction patterns, whose intensity ratio exhibits random distribution, the diffraction patterns of poled ceramics exhibit the characters of peak preference and anisotropic peak shift, due to the existence of texture and strain. With the aim to determine the phase structure in the PZT ceramics under electric field, it is important to eliminate these factors. Here, the Debye rings of diffraction pattern were divided into different azimuthal sectors with an interval of 15° to integrate the diffraction intensities, and the whole-pattern Rietveld method was employed to analyze the crystal structure [21]. Based on the refinement results, the diffraction patterns captured at the 45° sector, which is also 45° with respect to the electric field direction, have the minimum influence of texture. Thus, the detailed crystal structure of the PZT53.5 ceramics can be well resolved by in-situ diffraction under external electric field. This strategy to minimize the influence of texture is similar to the method reported by Hinterstein et al. [17,22].

Figure 1 shows the diffraction patterns obtained at the 45° sector as a function of electric field. As the electric field is below 1.0 kV/mm, the $(111)_{PC}$ and $(200)_{PC}$ peaks display negligible change [Fig. 1(c)], which implies no phase transition and domain switching. When the electric field exceeds 1 kV/mm, the $(200)_{PC}$ peaks exhibit a shift and an intensity change. This indicates a field-induced phase transition from the tetragonal phase to the monoclinic phase. The identification of the monoclinic phase will be discussed in the following paragraph. As the electric field exceeds 2.5 kV/mm, the $(111)_{PC}$ peaks split into two distinct peaks while the $(200)_{PC}$ reflections merge into a single one [Fig. 1(c) and (d)]. Interestingly, the tetragonal phase is completely transformed into the monoclinic phase. Moreover, neither the $(111)_{PC}$ nor $(200)_{PC}$ peaks change under the subsequent unloading of electric field [Fig. 1(e) and (f)]. Hence it can be concluded that the electric field induces the single monoclinic phase that persists also after the removal of the electric field. The above phenomenon is different from the previous observations in which the monoclinic phase coexists with the tetragonal or rhombohedral phases [10,17].

The presence of the single monoclinic phase can be confirmed by the full-pattern refinements. As shown in Fig. 2(a), the diffraction pattern of the PZT53.5 ceramic at 6 kV/mm is well refined by using single monoclinic phase (*Cm*) without introducing a preferential model. It gives the best refinement result, and the agreement R_{wp} factor is as low as 6.43% (Table S1). The possible presence of other phases is low, because worse refinements were obtained with the other phases, such as *P*4*mm* + *R*3*m*, *R*3*m*, and *Pm*, where the corresponding R_{wp} factor increased to 7.59%, 7.98%, and 7.10%, respectively. Furthermore, the existence of the single monoclinic phase is supported by the asymmetric character of the $(111)_{PC}$ and $(200)_{PC}$ peaks observed at the 0° sector [parallel to the electric field, Fig. S6(b)]. The asymmetric profiles indicate that more than one peak is present. The monoclinic phase exhibits two $(200)_{PC}$ reflection peaks. However, for the rhombohedral phase, the $(200)_{PC}$ profile is one and symmetric at every sector [23]. Accordingly, it can be confirmed from these results that the single monoclinic phase exists in the PZT53.5 ceramics.

Figure 2(b) shows the phase content of the tetragonal and monoclinic phases as a function of electric field. At low electric field (< 1 kV/mm), there is no phase transition. The major phase is the tetragonal one (64.1% probability) while the monoclinic phase exists with a probability of 35.9% (see Fig. S5 and Table S1).

Above 2.5 kV/mm, the tetragonal phase thoroughly transforms to the monoclinic phase. Notably, the electric field induced monoclinic phase remains stable, because the poled ceramic maintains the single monoclinic phase after removing the electric field [Fig. 2(b), and Fig. S4], and it is not altered with the subsequent change of bipolar electric field (Fig. S7).

It must be noted that the present single monoclinic phase of PZT53.5 was only observed in ceramics and not in powder. After the poled ceramics were crushed into powder, a small amount of monoclinic phase was transformed back to the tetragonal phase (Fig.S2). Moreover, the existence of a single monoclinic phase is also composition sensitive. In those compositions deviating from the MPB, such as PZT53 and PZT55, the monoclinic phase coexists with the tetragonal or rhombohedral phase. This is in agreement with the previous work of Guo *et al.*, in which the poled PZT52 ceramic showed the phase coexistence of tetragonal and monoclinic phases, while the poled PZT55 ceramic exhibited the coexistence of rhombohedral and monoclinic phases [10]. The findings of the present study can help to reveal the nature of the monoclinic phase in ceramics.

The spontaneous polarization (P_S) of the single monoclinic phase of PZT53.5 can be calculated by assuming standard atomic ionization states. The obtained P_S is 53 $\mu C/cm^2$ at 6 kV/mm. It is smaller than the spontaneous polarization theoretically predicted for the tetragonal composition of PZT50 near the MPB (76 $\mu C/cm^2$) [24]. The present calculated P_S is larger than the experimental maximum polarization (39 μC/cm^2) determined by hysteresis loops. Such discrepancy may be due to incomplete domain switching, direction deviation of P_S from electric field, and overestimated ionic valence of Pb, Ti, and Zr [25,26].

It is well-known that the piezoelectric response in ceramics is mainly ascribed to intrinsic lattice strain and extrinsic domain switching. In-situ SXRD can be used to explain the piezoelectric performance of the monoclinic phase [10,27-29]. The diffraction patterns captured at the 0° sector parallel to the electric field were utilized for extracting these contributions of the monoclinic phase. Here, we focus on the $(200)_{PC}$ peaks, in order to determine the different contributions from extrinsic domain switching and intrinsic lattice strain. The $(200)_{PC}$ profile was fitted by two peaks using the pseudo-Voigt function. The normalized relative volume fraction of switched domains, η_{norm}, is plotted in Fig. 3(a). For the monoclinic phase it is

$$\eta_{norm} = 3((I_{i,220M}/I_{0,220M})/(I_{i,220M}/I_{0,220M}+(I_{i,002M}/ I_{0,002M})/2)-2/3),$$

where I_0 is the initial intensity and I_i is the intensity of peaks under the applied electric field i. In the unpoled state the value of η_{norm} is 0, while in the saturated state η_{norm} is 1. For electric fields below 1.5 kV/mm, the domain switching of both tetragonal and monoclinic phases are negligible [Fig. 3(a)]. After the tetragonal phase is completely transformed to the monoclinic phase at 2.5 kV/mm [Fig. 2(b)], the monoclinic phase begins to show domain switching. As the electric field increases to the maximum value of 6 kV/mm, η_{norm} increases to 0.61. When the electric field is removed, η_{norm} slightly decreases and remains constant at a value of 0.57 in the remanent state (0 kV/mm). This indicates a unique property of negligible domain switching for the monoclinic phase. To quantify the motion of domains, we have evaluated the slope of normalized domain volume fraction, $\Delta\eta_{norm}/\Delta E$. The ratio $\Delta\eta_{norm}/\Delta E$ in the monoclinic phase is about 0.51 %/kV·cm^{-1}, that is much lower than that of the tetragonal and rhombohedral phases in the PZT. For example, the value of $\Delta\eta_{norm}/\Delta \mathrm{E}$ is 2.6 and 8.1 %/kV·cm^{-1} in the tetragonal PZT52 and La-doped PZT52, respectively [28]. In the rhombohedral phase of La-doped PZT60, $\Delta\eta_{norm}/\Delta E$ also reaches up to 1.47 %/kV·cm^{-1} [30]. Compared with the tetragonal and the rhombohedral phases, the monoclinic phase exhibits a striking property with a small reversible domain switching. This observation is helpful to analyze the contribution of intrinsic lattice strain to the piezoelectric response.

In order to quantify the intrinsic lattice strain contribution, the change of d_{220M} with electric field was determined. Figure 3(b) shows the relative lattice strain ε of the $(220)_M$ peak as a function of electric field, with ε defined as $\varepsilon = d_{i,220M}/d_{0,220M} - 1$, where d_i and d_0 are the d-spacing under an applied electric field i and the initial d-spacing, respectively. The change of lattice strain is consistent with the macro strain measured by the ferroelectric analyzer. The maximum lattice strain reaches as high as 0.28%, i.e. close to the macro strain of 0.32%. Notably, the reversible lattice strain, defined as the difference between maximum lattice strain and the remanent one, is 0.23%, and therefore is in very good agreement with the observed reversible macro strain (0.24%). From the value of ε, the extensional piezoelectric coefficient d_{33} and the transverse piezoelectric coefficient d_{31} are estimated to be 520 and -200 pm/V, respectively. These values are higher than those of PZT-4 (d_{33} = 300 pm/V, and d_{31} = -135 pm/V) and PZT-5A (d_{33} = 400 pm/V, and d_{31} = -185 pm/V), but lower than those of PZT-5H (d_{33} = 550 pm/V, and d_{31} = -250 pm/V) [31]. The present results show that the monoclinic phase exhibits large lattice strain during electrical loading. It is intriguing the fact that the intrinsic piezoelectric response of the single monoclinic phase is much larger than that of the single tetragonal or of the single rhombohedral one. For example, the d_{33} is 242 pm/V for the tetragonal phase in the PZT52 calculated from $(111)_{PC}$ and about 280 pm/V for the rhombohedral phase in the La-doped PZT60 calculated from $(200)_{PC}$, respectively [28,30]. Through the comparison with the first principle calculations, the predicted d_{33} value is much dependent on composition, which spans a large range from several hundreds to the maximum of ~4500 pm/V with increasing Zr content [12,13,16]. Such difference could be due to the fact that the present calculated d_{33} of the monoclinic phase was performed on polycrystalline ceramic in which the random orientation of grains, grain boundaries, local stress and other factors can restrict the piezoelectric performance.

Thus, the texture analysis demonstrates that the intrinsic lattice strain of the intermediate monoclinic phase is the main contribution to the piezoelectric response, while the contribution from the domain switching is negligible. The monoclinic phase, which possesses 24 polarizations and ferroelastic variants [32], facilitates the rotation of P_S under an applied electric field. This explains why the lattice strain of the monoclinic phase is sensitive to the electric field. In addition, the electric field induced phase transition to the monoclinic phase is consistent with the corresponding results from first principle calculations. Both demonstrate that the appearance of the monoclinic phase flattens the total free energies of tetragonal and rhombohedral phases around MPB [1,2,14] and that the monoclinic phase has a lower free energy under electric field loading. Therefore, the monoclinic plane of the tetragonal and rhombohedral phases around MPB can provide lower energy for the polar rotation, evidenced by the high piezoelectric response in the monoclinic plane as previously reported; the $(111)_{PC}$ shift of the La-doped PZT52 with major tetragonal phase and the $(200)_{PC}$ shift of the PZT55 with major rhombohedral phase are 460 pm/V and 500 pm/V, respectively [10,28,30]. Furthermore, it is interesting to study the fatigue performance of the monoclinic phase in the PZT, which can be investigated from the in-situ SXRD measurements on the crystal structure, the lattice strain, and the domain switching [22]. More details of in-situ SXRD studies on fatigue have been discussed in the Supplemental Material [21].

In conclusion, both the structural evolution and piezoelectric response of the PZT53.5 ceramics around the MPB have been investigated by in-situ high-energy SXRD. Structural refinements have been achieved at the 45° sector, which exhibits the minimum influence of texture. The tetragonal phase is completely transformed to the monoclinic phase which remains even stable under the subsequent loading of electric field. The monoclinic phase shows unique properties of large intrinsic strain and negligible domain switching, which play an important role in the mechanism of excellent piezoelectric properties near the MPB. The intrinsic lattice strain of the monoclinic phase is the primary cause of the macro strain in the PZT53.5 composition. The present results can be helpful for the understanding of the origin of excellent piezoelectric properties in other Pb or Pb-free MPB systems, as well as to study fatigue performance of ferroelectrics in future.

This work was supported by National Natural Science Foundation of China (Grant Nos. 21322102, 91422301, 21231001), Program for Changjiang Scholars and Innovative Research Team in University (IRT1207), the Fundamental Research Funds for the Central Universities, China (FRF-TP-14-012C1). Use of the Advanced Photon Source, an Office of Science User Facility operated for the U.S. Department of Energy (DOE) Office of Science by Argonne National Laboratory, was supported by the U.S. DOE under Contract No. DE-AC02-06CH11357.

[1] N. Huang, Z. Liu, Z. Wu, J. Wu, W. Duan, B. Gu, and X. Zhang, Phys. Rev. Lett. **91**, 067602 (2003).

[2] D. Damjanovic, Appl. Phys. Lett. **97**, 062906 (2010).

[3] B. Noheda, D. Cox, G. Shirane, J. Gonzalo, L. Cross, and S. Park, Appl. Phys. Lett. **74**, 2059 (1999).

[4] R. Haumont, B. Dkhil, J. M. Kiat, A. Al-Barakaty, H. Dammak, and L. Bellaiche, Phys. Rev. B **68**, 014114 (2003).

[5] B. Noheda, D. Cox, G. Shirane, J. Gao and Z. Ye, Phys. Rev. B **66**, 054104 (2002).

[6] J. Kiat, Y. Uesu, B. Dkhil, M. Matsuda, C. Malibert, and G. Calvarin, Phys. Rev. B,

65, 064106 (2002).

[7] Z. Ye, B. Noheda, M. Dong, D. Cox, and G. Shirane, Phys. Rev. B **64**, 184114 (2001).

[8] B. Noheda, D. Cox, and G. Shirane, R. Guo, B. Jones, and L. Cross, Phys. Rev. B **63**, 014103 (2000).

[9] B. Noheda and D. Cox, Phase Transitions **79**, 5 (2006).

[10] R. Guo, L. Cross, S. Park, B. Noheda, D. Cox, and G. Shirane, Phys. Rev. Lett. **84**, 5423 (2000).

[11] K. Oka, T. Koyama, T. Ozaaki, S. Mori, Y. Shimakawa, and M. Azuma, Angew. Chem. Int. Ed. **51**, 7977 (2012).

[12] L. Bellaiche, A. García, and D. Vanderbilt, Phys. Rev. B **64**, 060103 (2001).

[13] L. Bellaiche, A. García, and D. Vanderbilt, Ferroelectrics **266**, 377 (2002).

[14] H. Fu and R. Cohen, Nature, **403**, 281 (2000).

[15] M. Ahart, M. Somayazulu, R. Cohen, P. Ganesh, P. Dera, H. Mao, R. Hemley, Y. Ren, P. Liermann, and Z. Wu, Nature **451**, 545 (2008).

[16] L. Bellaiche, A. García, and D. Vanderbilt, Phys. Rev. Lett. **84**, 5427 (2000).

[17] M. Hinterstein, J. Rouquette, J. Haines, Ph. Papet, M. Knapp, J. Glaum, and H. Fuess, Phys. Rev. Lett. **107**, 077602 (2011).

[18] D. Phelan, X. Long, Y. Xie, Z. Ye, A. Glazer, H. Yokota, P. Thomas, and P. Gehring, Phys. Rev. Lett. **105**, 207601 (2010).

[19] Ragini, R. Ranjan, S. Mishra, and D. Pandey, J. Appl. Phys. **92**, 3266 (2002)

[20] B. Noheda, J. Gonzalo, L. Cross, R. Guo, S. Park, D. Cox, and G. Shirane, Phys. Rev. B **61**, 8687 (2000).

[21] See Supplemental Material at http://link.aps.org/supplemental/, which includes Refs. [22,**Error! Bookmark not defined.**], for additional information on sample fabrication, XRD data processing, determination of the monoclinic phase structure, discussions of the fatigue behavior and supporting figures.

[22] Last reference in Supplemental Material not already in Letter.

[23] Third reference in Supplemental Material not already in Letter.

[24] T. Qi, I. Grinberg, and A. Rappe, Phys. Rev. B **82**, 134113 (2010).

[25] Y. Kuroiwa, S. Aoyagi, A. Sawada, J. Harada, E. Nishibori, M. Takata, and M. Sakata, Phys. Rev. Lett. **87**, 217601 (2001).

[26] R. Cohen, Nature **358**, 136 (1992).

[27] G. Tutuncu, B. Li, K. Bowman, and J. Jones, J. Appl. Phys. **115**, 144104 (2014).

[28] A. Pramanick, J. Daniels, and J. Jones, J. Am. Ceram. Soc. **92**, 2300 (2009).

[29] G. Tutuncu, L. Fan, J. Chen, X. Xing, and J. Jones, Appl. Phys. Lett. **104**, 132907 (2014).

[30] A. Pramanick, D. Damjanovic, J. Daniels, J. Nino, and J. Jones, J. Am. Ceram. Soc. **94**, 293 (2011).

[31] A. Safari, E. Akdoğan, *Piezoelectric and Acoustic Materials for Transducer Applications* (Springer, Berlin, Heidelberg, 2008), p. 226.

[32] J. Li, R. Rogan, E. Üstündag, and K. Bhattacharya, Nat. Mater. **4**, 776 (2005).

Figure Captions

FIG. 1. (a) The schematic of experimental geometry. (b) Selected diffractions from different sector at the first quadrant. The 0° and the 90° sector are parallel and perpendicular to electric field, respectively. (c-f) The in-situ evolution of $(111)_{PC}$ and $(200)_{PC}$ reflections at the 45° sector as function of electric field. (c) is for the electric loading, while (e) for the electric unloading. (d) and (f) are contour plots of diffraction intensities of $(111)_{PC}$ and $(200)_{PC}$ reflections, which are the projection of (c) and (e), respectively.

FIG. 2. (a) Structural refinement results of PZT53.5 at 6 kV/mm. The black asterisks indicate the raw diffraction data, red line corresponds to the calculated diffraction pattern, and the blue vertical ticks mark the calculated positions of *Cm* phase reflections. The insets show the enlarge profile of $(111)_{PC}$ and $(200)_{PC}$ reflections. (b) Phase fraction of the tetragonal and monoclinic phases as function of electric field. The error bars are smaller than the symbols.

FIG. 3. (a) The influence of electric field on normalized relative domain fraction, η_{norm}, of the monoclinic and tetragonal phases. (b) Relative lattice strain of $(200)_{PC}$ reflection, ε, of the monoclinic phase and the macro strain measured by the ferroelectric analyzer for the PZT53.5 ceramic as function of electric field.

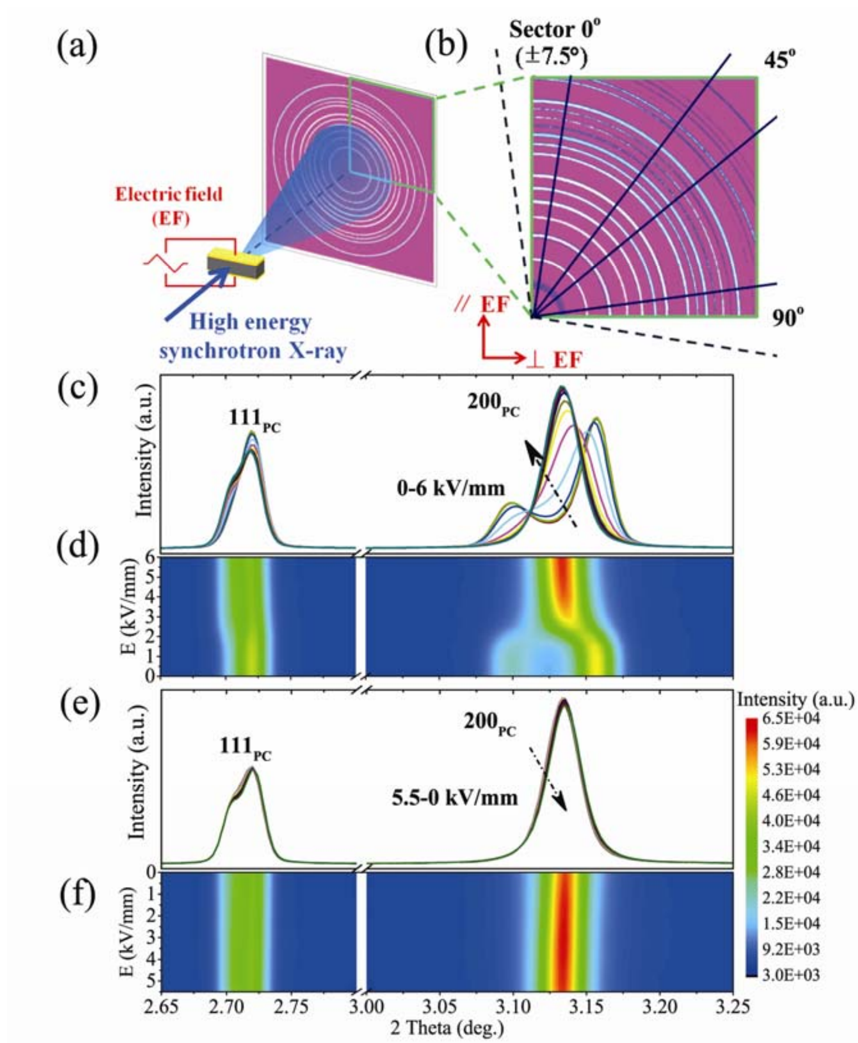
(a)
(b)
Sector 0°
(±7.5°)
45°
90°
Electric field
(EF)
High energy
synchrotron X-ray
// EF
⊥ EF
(c)
111PC
200PC
0-6 kV/mm
Intensity (a.u.)
(d)
E (kV/mm)
(e)
111PC
200PC
5.5-0 kV/mm
Intensity (a.u.)
(f)
E (kV/mm)
Intensity (a.u.)
6.5E+04
5.9E+04
5.3E+04
4.6E+04
4.0E+04
3.4E+04
2.8E+04
2.2E+04
1.5E+04
9.2E+03
3.0E+03
2.65 2.70 2.75 3.00 3.05 3.10 3.15 3.20 3.25
2 Theta (deg.)

FIG. 1

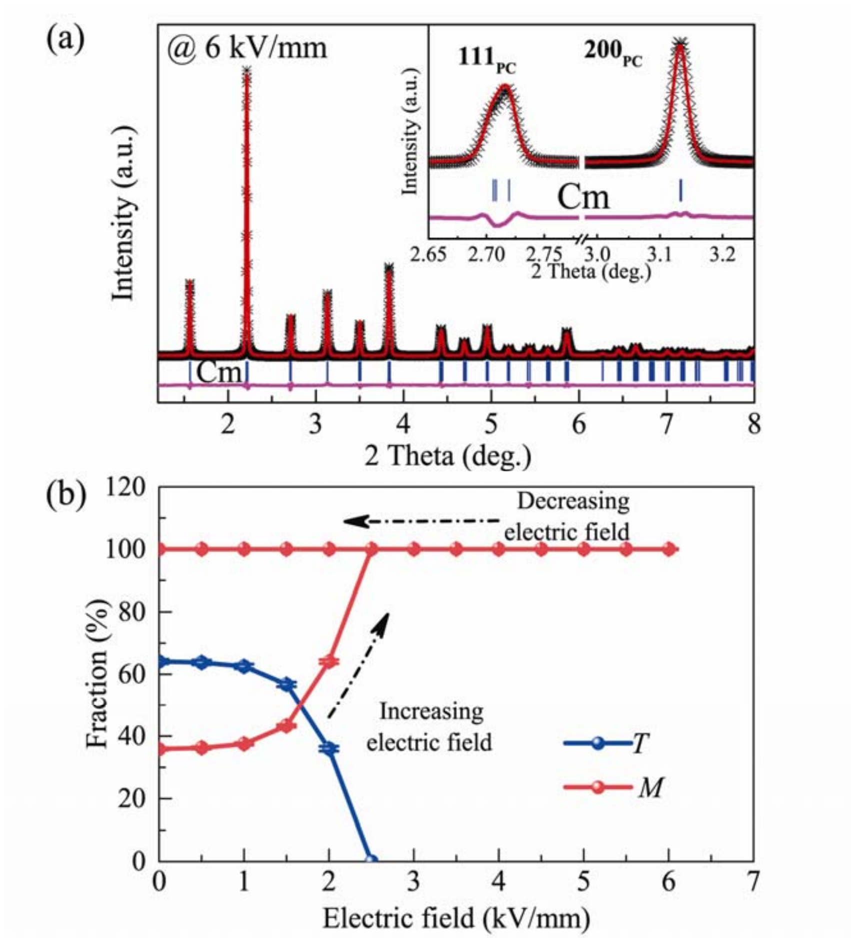

(a)
@ 6 kV/mm
Intensity (a.u.)
Cm
2 Theta (deg.)
111PC
200PC
Intensity (a.u.)
Cm
2.65 2.70 2.75 3.0 3.1 3.2
2 Theta (deg.)
2 3 4 5 6 7 8
(b)
Fraction (%)
0 20 40 60 80 100 120
Decreasing electric field
Increasing electric field
T
M
0 1 2 3 4 5 6 7
Electric field (kV/mm)

FIG. 2

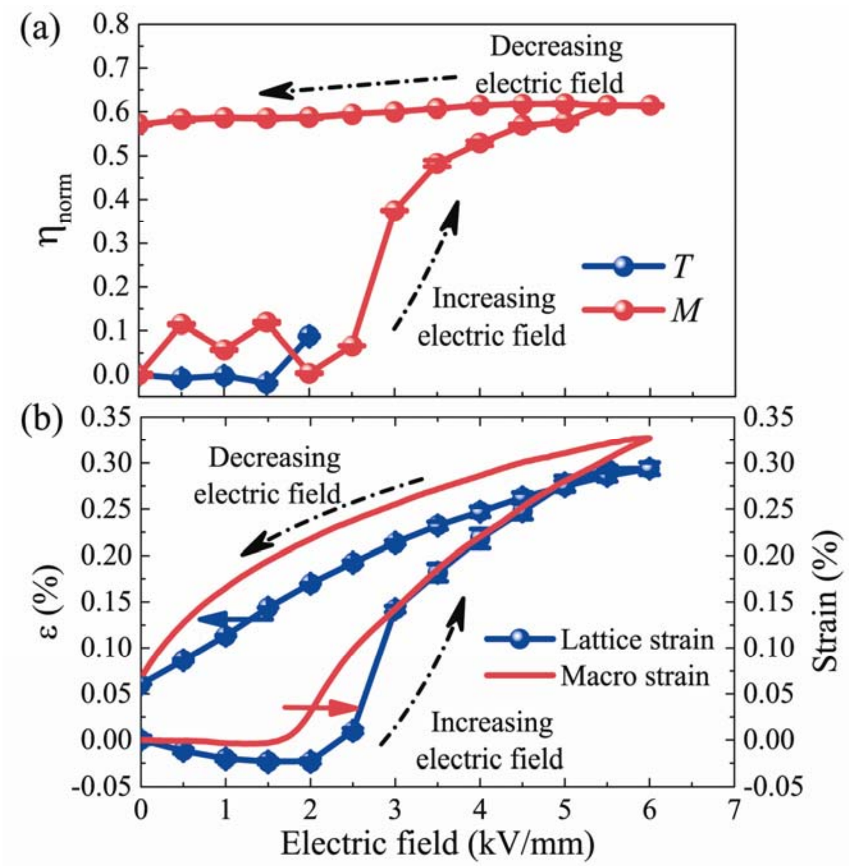
(a)
Decreasing
electric field
Increasing
electric field
η_norm
T
M
(b)
Decreasing
electric field
Increasing
electric field
ε (%)
Strain (%)
Lattice strain
Macro strain
Electric field (kV/mm)

FIG. 3